Available online at www.sciencedirect.com
ScienceDirect
International Journal of Heat and Mass Transfer 51 (2008) 3803–3815
International Journal of HEAT and MASS TRANSFER
www.elsevier.com/locate/ijhmt

On the double-layer structure of the boundary layer adjacent to a sidewall of a differentially heated cavity

Feng Xu *, John C. Patterson, Chengwang Lei

School of Engineering, James Cook University, Townsville, QLD 4811, Australia

Received 19 August 2007; received in revised form 10 January 2008
Available online 7 March 2008

Abstract

This study is concerned with the transition of the boundary layer adjacent to a sidewall of a differentially heated cavity to a double-layer structure and with the important flow and heat transfer features of the double-layer structure. The transition to the double-layer structure is examined by comparing numerical and experimental results. The mechanism responsible for the formation of the double-layer structure, i.e. the stratification of the fluid in the core, is discussed. Detailed discussion of the energy balance adjacent to the sidewall reveals that the heat transfer in the double-layer structure is rather complex. There is an opposing horizontal thermal diffusion within the double-layer structure.

Keywords: Boundary layer; Double-layer structure; Stratification; Heat transfer

1. Introduction

Fluid motions induced by a vertical heated or cooled boundary are common in nature [1], and are relevant to industrial systems such as electronic cooling, heat exchangers, crystal growth procedures and many other applications. In particular, studies of the boundary layer flow adjacent to a vertical sidewall of a differentially heated cavity have been extensively reported [2,3].

In early studies of natural convection in a differentially heated cavity, considerable attention has been given to natural convection flows at the steady state. Batchelor [4] indicated that, for a small Rayleigh number in a tall cavity, conduction dominated the heat transfer through the cavity, and suggested that the fluid in the core was isothermal. However, later on, the existence of a stratification of the fluid in the core was demonstrated by Eckert and Carlson [5] using an interferometer; and a 'cats-eye' flow pattern in a tall cavity was visualized by Elder [2]. Based on a stratified core, analytical solutions of the boundary layer in the cavity were obtained by Elder [2] and Gill [3], respectively. These reported experiments and analytical solutions of the boundary layer flow in the cavity are also consistent with the double-layer flow structure adjacent to a heated wall in a stratified fluid ambient [1,6–9], in which a temperature deficit and velocity reversal are observed.

Transient flows in a differentially heated cavity have also been studied and reported extensively in the literature due to their relevance to many applications. Analytical solutions of the transient flow resulting from sudden heating of a vertical wall were obtained [10,11]. It has been demonstrated that, following sudden heating, small perturbations referred to as the leading edge effect (LEE, [12–14]) arise in the vicinity of the leading edge and propagate downstream. The LEE propagation is an important transient feature of the boundary layer following sudden heating in that it appears to be the mechanism by which the flow changes from one-dimensional and unsteady [8,15] to two-dimensional and steady [16], and thus the speed at which the LEE travels became the focus of many earlier reports [12]. However, the theoretical predictions of the LEE propagation speed by [11,17] were not supported by experimental measurements and numerical results [18–20]. Armfield

* Corresponding author. Tel.: +61 747814420; fax: +61 747816788.
E-mail address: feng.xu@jcu.edu.au (F. Xu).

0017-9310/$ - see front matter © 2008 Elsevier Ltd. All rights reserved.
doi:10.1016/j.ijheatmasstransfer.2008.01.005

Nomenclature

A	aspect ratio, H/L	ΔT	temperature difference between two sidewalls (K)
g	acceleration due to gravity (m/s^2)	u, v	velocity components in the x and y directions (m/s)
H, L	height and length of the cavity (m)	x, y	horizontal and vertical coordinates (m)
p	pressure (N/m^2)	β	coefficient of thermal expansion (1/K)
Pr	Prandtl number, ν/κ	κ	thermal diffusivity (m^2/s)
Ra	Rayleigh number, $g\beta\Delta TH^3/\nu\kappa$	ν	kinematic viscosity (m^2/s)
t	time (s)	ρ	density (kg/m^3)
T	temperature (K)		
T_m	reference temperature (K)		

and Patterson [13] used stability analyses to show that the LEE propagation speed may be predicted by the maximum speed of the travelling waves in the boundary layer induced by initial perturbations. This proposition was also supported by the experimental results reported in [14].

After the passage of the LEE, the boundary layer flow becomes stable for Rayleigh numbers below a critical value. In this stable stage, the presence of the horizontal ceiling of the cavity forces a horizontal intrusion into the central part of the cavity [21]. The intrusion may exhibit separation from the ceiling and trailing waves [22–25]. In the subsequent development of the cavity flow in which the far wall is cooled, the intrusion ultimately reaches the opposing wall and a cavity-scale oscillation may arise [26]. In a shallow cavity (i.e. with an aspect ratio less than unity), the oscillation may be strong enough to result in a reverse flow which moves back to the hot wall and splits the hot intrusion into two streams [26], with an upper stream moving toward the cold wall along the ceiling and a lower stream discharging into the core. The reverse flow may result in an instability of the lower stream, which is of a different character from the instability present in the boundary layer [27].

The above-mentioned transient development of the boundary layer flow based on numerical results has been partly supported by the experimental observations of Xu et al. [28], in which the transition of the boundary layer adjacent to the sidewall from start-up to a steady state was classified into three stages based on kinematic flow properties: an initial growth stage, an entrainment development stage and a steady stage. In the initial stage, distinct kinematic properties include the growth of the boundary layer and the LEE propagation. In the entrainment development stage, the horizontal intrusion and entrainment by the vertical boundary layer are dominant and may persist for a relatively long period. In the steady stage, a double-layer structure of the vertical boundary layer is visualized in shadowgraph images.

As can be seen from the above review, the early-stage development of the boundary layer flow adjacent to the sidewall of the differentially heated cavity (e.g. the LEE) is very similar to that adjacent to a heated vertical wall immersed in an ambient fluid, which has been well described in the literature [12–14,21]. Furthermore, the flow structure in the steady state has also been discussed extensively [2,3]. However, the transitional process of the fluid in the core from an initially isothermal state to a thermally stratified structure at the steady state has been rarely reported except in [29,30], and few studies have considered the relationship between the development of the boundary layer on the sidewall and the stratification of the fluid in the core. Although the evolution of the double-layer structure of the boundary layer on the sidewall was previously reported by the present authors [28], the mechanism responsible for its formation and its dynamic and thermal features could not be confirmed due to limitations of the shadowgraph technique. Furthermore, the relationship between the double-layer structure observed in the shadowgraph images and the reported temperature deficit and flow reversal which occurs in the boundary layer in a stratified ambient at the steady state [3] remains unresolved. Therefore, a further joint numerical and experimental study, which enables a detailed investigation and thorough understanding of various aspects of the development of the double-layer structure, is motivated.

In this paper, the focus is on the relationship between the double-layer structure of the boundary layer on the sidewall observed in shadowgraph images and the stratification of the fluid in the core, as well as the flow and heat transfer properties of the double-layer structure. In the remainder of this paper, the experimental setup and numerical procedures are described in Section 2. Based on comparisons between numerical simulations and shadowgraph observations, the formation of the double-layer structure is characterized, and the mechanism responsible for the formation of the double-layer structure is described in Section 3. Finally, the flow and heat transfer features of the double-layer flow structure are discussed in Section 4, and conclusions are presented in Section 5.

2. Experimental setup and numerical procedures

2.1. Experimental setup

The experimental setup is shown in Fig. 1a. Briefly, the inner dimensions of the cavity containing water as the

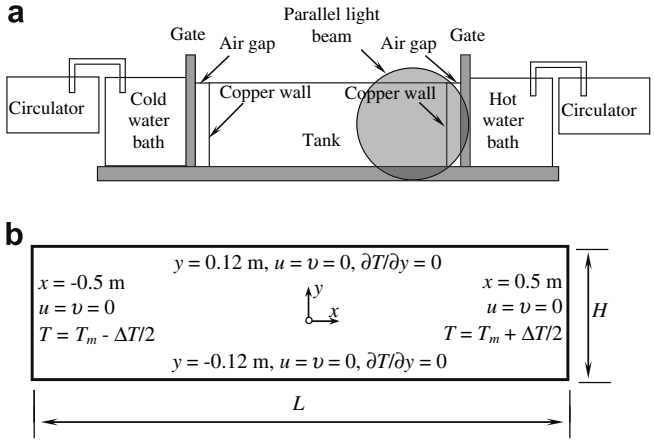

Fig. 1. (a) Schematic of the experimental setup, and (b) physical domain and boundary conditions for numerical simulations.

working fluid are $H = 0.24$ m (height), $L = 1$ m (length) and $W = 0.5$ m (width), and the cavity is made of 0.019 m thick Perspex sheets except for the heated and cooled sidewalls, which are constructed from 0.24×0.5 m gold-coated copper plates of 0.00113 m thickness. Two constant-temperature water baths are used to heat and cool the sidewalls. Each water bath, connected to a refrigerated/heating circulator, is separated from the sidewall by a pneumatically operated gate with an air gap between the gate and sidewall, as seen in Fig. 1a. When the experiment starts, the pneumatic gates are lifted rapidly so that the hot or cold water in the water baths floods against the copper sidewalls of the cavity, providing a very fast isothermal boundary at each end of the cavity, as described in [31,32]. Due to the symmetry of the flows adjacent to the two sidewalls, the flow adjacent to the heated sidewall (on the right) is the focus of this paper. Further details regarding the experimental setup are given in [28] and earlier papers [31,32].

The boundary layer flow adjacent to the sidewall is visualized using a shadowgraph technique, the implementation of which in this experiment has been described in detail elsewhere [28,32]. It is well known that the intensity variation of the shadowgraphs is approximately sensitive to the second derivative of temperature [33], and thus bright strips in shadowgraph images correspond to the minima or maxima of the second derivative of temperature in the direction normal to the strip. This correspondence is subject to the assumptions that the temperature variation in the direction in which the light beam enters the flow field may be neglected (that is, the flow is approximately two-dimensional), and the overall deflection of the light rays is sufficiently small.

2.2. Numerical procedures

It has been demonstrated previously that two-dimensional numerical simulations may characterize well the transient natural convection flows in a differentially heated cavity at Rayleigh numbers relevant to the present study (10^8–10^{10}, see e.g. [31,34]). Therefore, a two-dimensional rectangular domain (see Fig. 1b), which is 0.24 m (H) by 1 m (L), is adopted for the present numerical simulation, based on the experimental model shown in Fig. 1a. The two-dimensional Navier–Stokes and energy equations with the Boussinesq approximation to be solved in this study are expressed as follows,

$$\frac{\partial u}{\partial x} + \frac{\partial v}{\partial y} = 0, \tag{1}$$

$$\frac{\partial u}{\partial t} + u\frac{\partial u}{\partial x} + v\frac{\partial u}{\partial y} = -\frac{1}{\rho}\frac{\partial p}{\partial x} + \nu\left(\frac{\partial^2 u}{\partial x^2} + \frac{\partial^2 u}{\partial y^2}\right), \tag{2}$$

$$\frac{\partial v}{\partial t} + u\frac{\partial v}{\partial x} + v\frac{\partial v}{\partial y} = -\frac{1}{\rho}\frac{\partial p}{\partial y} + \nu\left(\frac{\partial^2 v}{\partial x^2} + \frac{\partial^2 v}{\partial y^2}\right) + g\beta(T - T_{\mathrm{m}}), \tag{3}$$

$$\frac{\partial T}{\partial t} + u\frac{\partial T}{\partial x} + v\frac{\partial T}{\partial y} = \kappa\left(\frac{\partial^2 T}{\partial x^2} + \frac{\partial^2 T}{\partial y^2}\right). \tag{4}$$

For the purpose of comparing the numerical results with the experimental measurements, the same flow and temperature conditions as those of the experiment are considered in the numerical simulations. Initially, the fluid in the cavity is motionless and isothermal at a temperature T_{m}. At time $t = 0$, the two sidewalls are abruptly heated and cooled, respectively, while the top and bottom walls are both insulated, as shown in Fig. 1b. In this study, the reference temperature (T_{m}) and the temperature difference between the two sidewalls (ΔT) are 295.55 K and 16 K, respectively. The corresponding controlling parameters include the Rayleigh number ($Ra = 3.77 \times 10^9$), Prandtl number ($Pr = 6.64$) and aspect ratio ($A = 0.24$).

Eqs. (1)–(4) are solved using a finite-volume method with the SIMPLE scheme, where the convection term is discretized with a second-order upwind scheme and the diffusion term with a second-order center-differenced scheme. A hybrid grid system is constructed with finer non-uniform grids distributed in the vicinity of all the wall boundaries (a zone of 0.05 m adjacent to the walls) and uniform grids in the central region of the flow domain in order to accurately capture the features of the boundary layer flow. A mesh dependence test has been conducted using two different meshes (395×1155 and 199×563). Fig. 2a shows typical time series of the calculated temperatures at a point near the downstream end of the boundary layer (0.498, 0.09 m) with the two meshes. A logarithmic scale plot of the same temperature series is presented in Fig. 2b in order to compare the early-stage flow features with the two meshes. It is seen in Fig. 2 that the calculated temperatures with the two meshes are consistent with each other throughout all stages of the flow development (from the start-up to the steady state), and minor variations between the two meshes are discernible only at the presence of waves. This indicates that the overall development of the basic flow, except for the details of the waves (convective instability, refer to [6,7]), is independent of the adopted

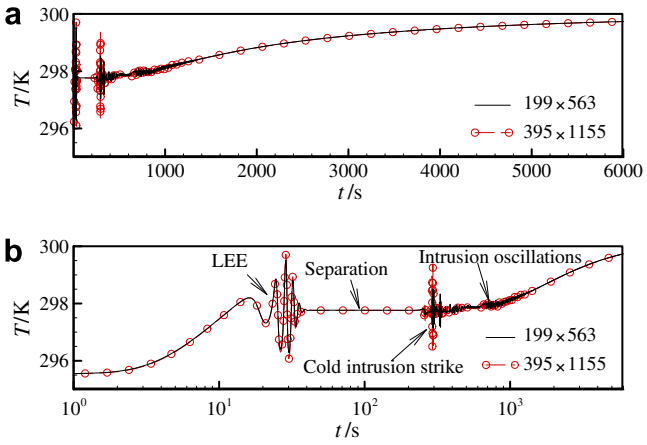

Fig. 2. Time series of the temperature at (0.498, 0.09 m) with different meshes. (a) Linear time scale, and (b) logarithmic time scale.

mesh. Therefore, in consideration of the computing time, the coarser mesh of 199 (H) × 563 (L) is adopted. This mesh has a grid inflation factor of 1.04 toward the centre of the domain in both the horizontal and vertical boundary zones and the smallest grids of 0.00016 × 0.00016 m located at the four corners.

Time marching is carried out by a second-order implicit scheme. Time-step-dependence tests were carried out with two time-steps of 0.1 and 0.05 s, respectively. For the two cases with different time-steps, there is no discernible difference in the calculated temperature and flow fields. Therefore, the time-step of 0.1 s is considered to be sufficiently small for capturing the major flow features.

3. Transition of the boundary layer to a double-layer structure

The overall transition of the boundary layer flow may be characterized as follows: In the very early-stage, the boundary layer is one-dimensional and the temperature signal at a fixed vertical position follows the growth described by Goldstein and Briggs [11]. However, the presence of the leading edge is felt with the arrival of the LEE, resulting in an instability of the boundary layer, as indicated by the first group of traveling waves in Fig. 2b [12–14]. After the LEE perturbations travel downstream, the boundary layer flow becomes steady [16] until the arrival of the cold intrusion flow from the opposing sidewall. Previous investigations [22–24] show that separation of the horizontal intrusion happens at this stage, which is also marked in Fig. 2b. When the cold intrusion from the opposing sidewall strikes the hot wall, it may trigger a convective instability of the boundary layer, as indicated by the second group of traveling waves in Fig. 2b [31]. At a certain stage after the arrival of the intrusion from the opposing sidewall, the intrusion flow oscillates, and as a consequence, a reverse flow resulting from the intrusion oscillation induces an instability of the lower stream of the intrusion, which is represented by the third group of waves in Fig. 2b (also see [27]). Eventually the boundary layer flow enters a slow evolution process toward the steady state, as indicated by a smooth increase of the temperature in Fig. 2a (for $t > 1500$ s).

3.1. Formation of the double-layer structure

For the early development of the transient natural convection flow in the cavity following sudden heating, comparisons between numerical and experimental results may be found in [31]. Fig. 3 shows comparisons between the shadowgraphs and the isotherms generated in the numerical simulation at the time when the cold intrusion, marked by the solid line overdrawn at the bottom of Fig. 3a, is approaching the hot wall. Fig. 3a is a processed shadowgraph image in which a background image recorded immediately before the start of the experiment is subtracted from the original shadowgraph image. The same image processing procedure is applied to all shadowgraph images shown in subsequent figures. Fig. 3b plots the corresponding isotherms of the numerical simulation at the same stage of the flow development. It is seen in this figure that the shadowgraph pattern and isotherms adjacent to the sidewall (including the boundary layer flow and the cold intrusion head) are very similar. However, the numerically generated downstream corner flow remains stable, in contrast to the unstable experimental flow. We also compare the numerical results obtained with different meshes, and find that the corner flow structures calculated with different meshes are very similar, suggesting that the presence of various perturbations in the experiment leads to the destabilization of a roll structure in the top corner (refer to [28]). Furthermore, the streamlines shown in Fig. 3c imply that the entrainment into the boundary layer is entirely from the cold intrusion at this time, rather than from the fluid discharged at the downstream end of the boundary layer, which is the case at earlier times (see [31]).

It is worth noting that the development of the calculated flow is faster than that observed in the experiment. Patterson and Armfield [31] suggested that the timing difference is a result of achieving a smaller Rayleigh number in the experiment than that in the numerical simulation (approximately 80% of the Rayleigh number specified numerically). This is explained as follows: Although the water in the hot water bath is stirred, a thermal boundary layer may still form on the water bath side of the sidewall, resulting in a lower temperature on the heated sidewall than the average water temperature in the hot water bath. Similarly, the temperature of the cooled sidewall is higher than the average water temperature in the cold water bath. Accordingly, the actual temperature difference between the two sidewalls is smaller than that between the two water baths. This means that the Rayleigh number achieved in the experiment is slightly smaller than that calculated if the sidewall temperatures are approximated by the average water temperatures in the water baths. As a consequence, the development of the calculated flow at a slightly higher Rayleigh

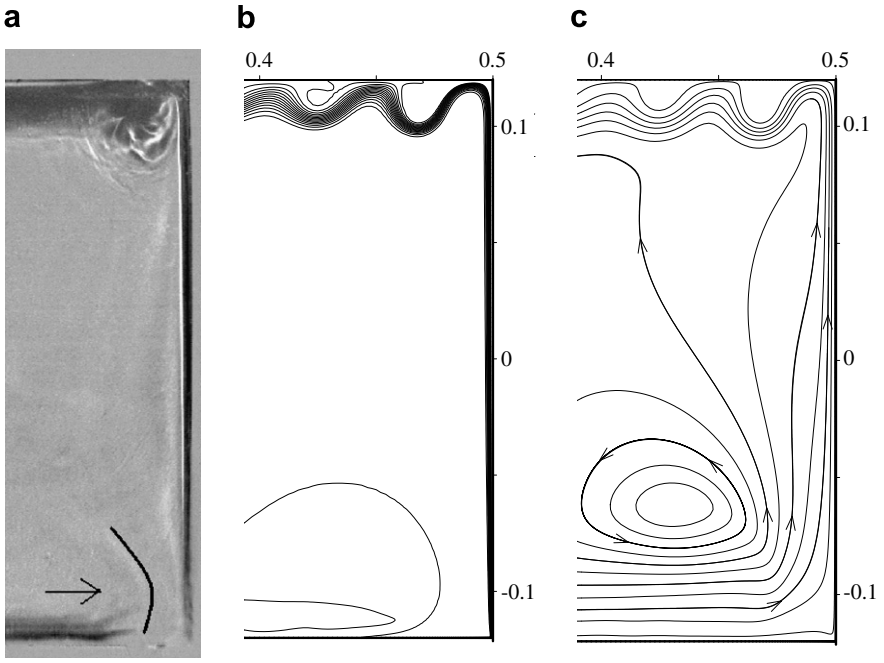

Fig. 3. The arrival of the cold intrusion at the hot wall. (a) Shadowgraph image at $t = 335$ s, (b) isotherms at $t = 235$ s (contours between 295.23 and 300.19 K with an interval of 0.31 K), and (c) streamlines at $t = 235$ s (contours between 1.77×10^{-5} and 1.95×10^{-4} m^2 s^{-1} with an interval of 1.77×10^{-5} m^2 s^{-1}).

number is faster than that of the experimentally visualized flow. However, since the subsequent development of the boundary layer flow is a slow transition to the steady state, as indicated by the temperature plot in Fig. 2, the timing difference between the experiment and numerical simulation becomes less significant. Therefore, in the following figures the experimental and numerical results at the same time are compared.

Fig. 4 shows the subsequent development of the vertical boundary layer after the cold intrusion strikes the hot wall. It is seen in the shadowgraph image that a second bright strip arises near the upstream corner outside the thermal

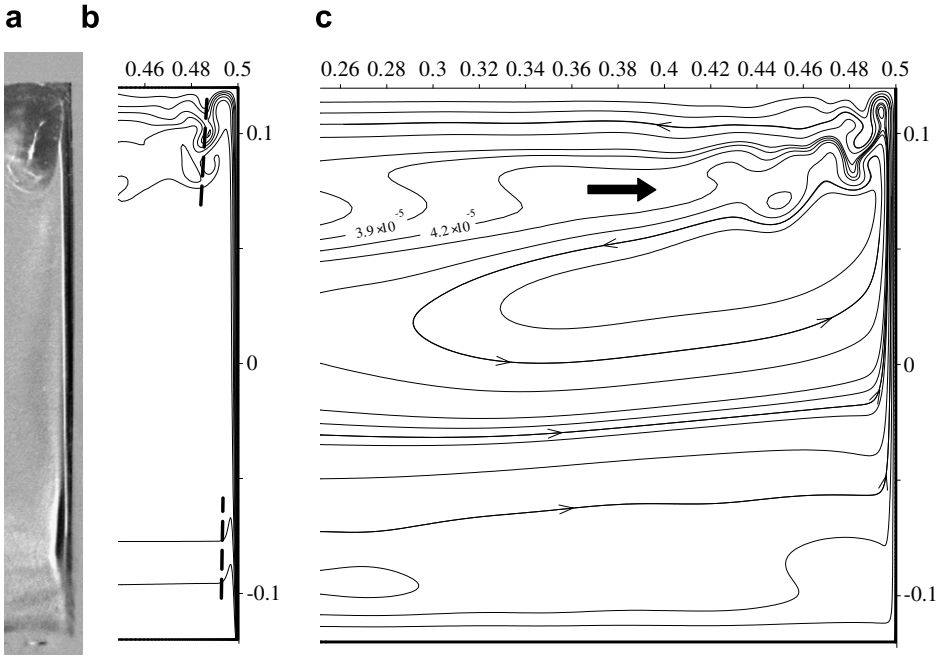

Fig. 4. Appearance of the double-layer structure at $t = 695$ s. (a) Shadowgraph image, (b) isotherms (solid lines showing contours between 294.1 and 301.1 K with an interval of 1 K) and lines of the minimum second derivative of temperature (dashed lines), and (c) streamlines (unlabeled contours between 6.70×10^{-6} and 6.70×10^{-5} m^2 s^{-1} with an interval of 7.50×10^{-6} m^2 s^{-1}).

(inner) boundary layer (marked by the bright strip closest to the wall). Likewise, a similar bright strip is also noticeable in the downstream corner. These two outer bright strips correspond to the computed positions of the minima of the second derivative of temperature (indicated by the dashed lines in Fig. 4b). Note that the second derivative of temperature here denotes $\partial^2 T/\partial x^2$, because $\partial^2 T/\partial y^2$ is negligibly small in the vertical boundary layer, consistent with the observation that the strips are approximately parallel to the vertical wall. It is seen in Fig. 4b that an upward thermal tongue of isotherms close to the sidewall (with fluid colder than that on both sides, resulting in a temperature deficit in the region) is present near the upstream corner, and is fed by the incoming cold intrusion. The streamlines in Fig. 4c display that a reverse flow resulting from the cavity-scale intrusion oscillation, indicated by the overdrawn arrow, splits the hot intrusion into two parts, an upper part that moves to the cold wall under the ceiling and a lower part that discharges into the cavity and forms a circulation, trapping cold fluid between itself and the boundary layer.

Fig. 5 shows further development of the boundary layer flow. Clearly, both the upper and lower outer bright strips extend further toward the mid height as time increases. The corresponding isotherms in Fig. 5b indicate that the hot and cold intrusions have grown thicker, and both the upper and lower upward thermal tongues have also extended further toward the mid height. The two outer bright strips eventually meet at the mid height of the cavity as the flow continues to develop, which is shown in Fig. 5c. It is evident in Fig. 5c that the two outer bright strips meet near the mid height. It is evident in this figure that the two bright strips do not align vertically, with the descending bright strip further away from the hot wall than the ascending one. It is also seen from the numerical isotherms that the upward thermal tongue in the upper part of the cavity is much greater than that in the lower part (Fig. 5d), and a circulation, driven by the misalignment, is clearly present around the meeting point of these two outer bright strips (Fig. 5e).

Compared with the flow structures shown in Fig. 5c, the two outer bright strips at a very much later time as shown in Fig. 6a have aligned vertically and a continuous outer layer has formed. The corresponding isotherms in Fig. 6b indicate that the width of the upward thermal tongue decreases continuously from the top to the bottom. Fig. 6c shows that the circulation around the mid height is split into two smaller circulations. The temperature and flow structures within the double-layer structure at this time are better viewed from the horizontally enlarged plots shown in Fig. 6d and e, and will be further discussed in Section 4.

It is worth noting that the double-layer structure observed in the shadowgraph images does not correspond exactly to the vertical boundary layer flow and flow reversal observed by Elder [2] (see Section 4 for further discussion). As mentioned previously, the outer bright strips (refer to Figs. 4a, 5a and 6a) correspond to the position

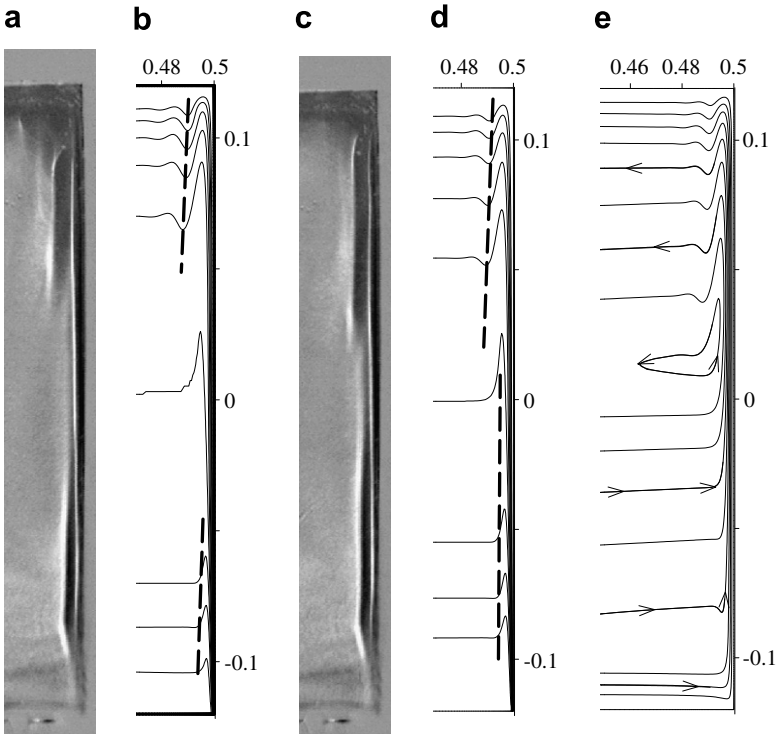

Fig. 5. Development of the double-layer structure. (a) Shadowgraph image at $t = 1500$ s, (b) isotherms (solid lines showing contours between 292.55 and 300.55 K with an interval of 1 K) and lines of the minimum second derivative of temperature (dashed lines) at $t = 1500$ s, (c) Shadowgraph image at $t = 2500$ s, (d) isotherms (solid lines showing contours between 292.55 and 300.55 K with an interval of 1 K) and lines of the minimum second derivative of temperature (dashed lines) at $t = 2500$ s, and (e) streamlines (contours between 3.30×10^{-6} and 3.33×10^{-5} m^2 s^{-1} with an interval of 3.30×10^{-6} m^2 s^{-1}) at $t = 2500$ s.

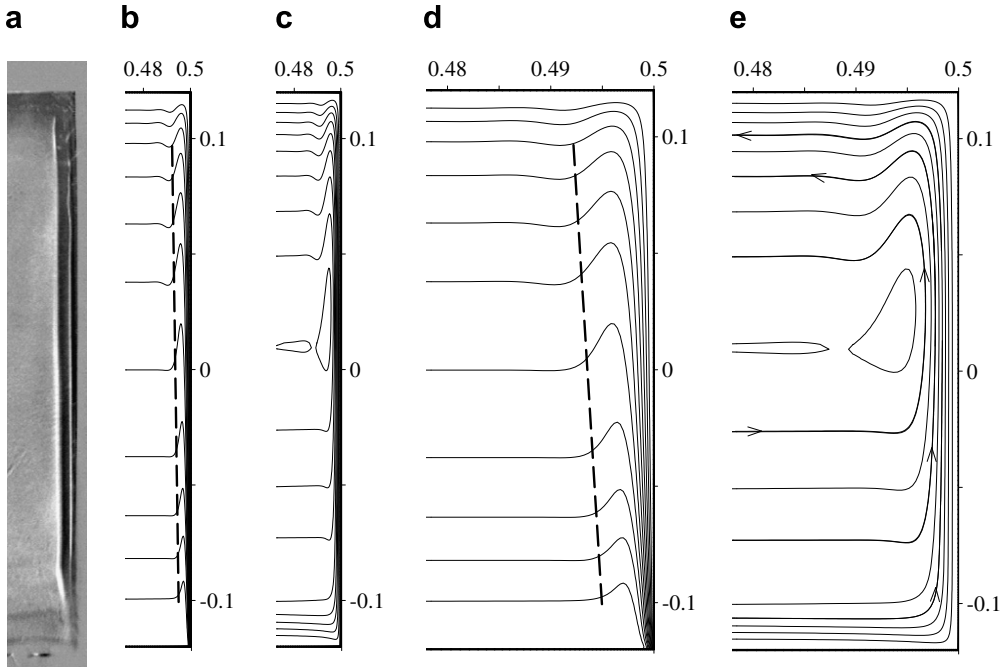

Fig. 6. Double-layer structure at $t = 4700$ s. (a) Shadowgraph image, (b) isotherms (solid lines showing contours between 291.55 and 301.55 K with an interval of 1 K) and lines of the minimum second derivative of temperature (dashed lines), (c) streamlines (contours between 2.50×10^{-6} and 2.46×10^{-5} m^2 s^{-1} with an interval of 2.80×10^{-6} m^2 s^{-1}), (d) horizontally enlarged plot of (b), and (e) horizontally enlarged plot of (c).

Table 1
Positions of the computed maxima and minima of the second derivative of temperature and the observed bright strips in the shadowgraph image at $t = 4700$ s

Location	Distance measured from the hot wall (m)			
y (m)	Computed $\left.\frac{\partial^2 T}{\partial x^2}\right\|_{max}$	Inner bright strip	Computed $\left.\frac{\partial^2 T}{\partial x^2}\right\|_{min}$	Outer bright strip
−0.06	0.0014	0.0023	0.0054	0.0069
0.06	0.002	0.0032	0.0075	0.0087

of the minima of the second temperature derivatives [33], the computed positions of which are shown with dash-dotted lines in Figs. 4b, 5b, and 6b. Quantitative comparisons between the computed positions of the maxima and minima of the second derivative of temperature and the observed positions of the two bright strips in the shadowgraph image shown in Fig. 6 are given in Table 1. The positions shown in Table 1 are measured as the distance from the hot wall. It is seen that the predicted positions compare well with the observations, but are consistently smaller than the observed values. This is also attributed to the hypothesis that the experiment achieved a Rayleigh number lower than that specified in the numerical simulation.

3.2. Double-layer structure and stratification of the fluid in the core

The presence of a temperature deficit and flow reversal of the vertical boundary layer adjacent to an isothermal wall in a stratified medium has been noted [1,3,6–8,35]. These studies have been either in the context of a differentially heated cavity, in which case the stratification is the final steady state condition in the core, or a plate immersed in a stratified ambient, in which case the stratification is imposed. It is clear that the temperature deficit and flow reversal are linked to the ambient stratification; simulations of an isothermal wall in an unstratified medium show no indication of these features [13]. However, the mechanisms have not been discussed from a physical point of view, nor linked to the transient development of the flow. They are discussed below in the content of transient flow development.

At an early time (Fig. 4, $t = 695$ s), there is no interior stratification with the exception of the effects of the incoming cold intrusion from the far wall at the lower boundary of the cavity, and the complex structures near the ceiling. This is confirmed by the vertical temperature profiles along the center line of the cavity plotted in Fig. 7. Although there is some evidence of a reverse flow and a temperature deficit (corresponding to the upward thermal tongue in Figs. 4b, 5b and 6b) in the latter case, this is clearly a result of the discharge being deflected away from the ceiling. On the other hand, there is clear evidence of a temperature deficit at the lower end, over the range of the stratification induced by the incoming intrusion.

At a later time (e.g. $t = 1500$ s), the interior stratification has extended over approximately one quarter of the cavity depth (also see Fig. 7) from both the floor and the ceiling, as a consequence of the filling from the discharges from both vertical boundary layers. The apparent temperature deficit shown in Fig. 5b at the mid height is in a region of an extremely small temperature gradient, and the actual

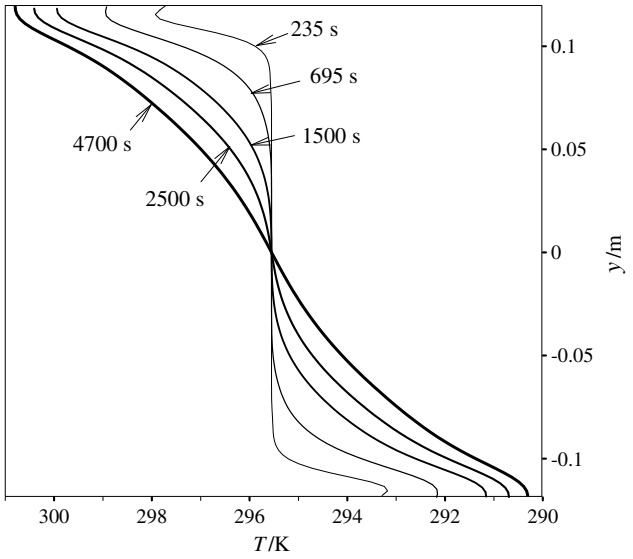

Fig. 7. Vertical temperature profiles along the centerline at different times.

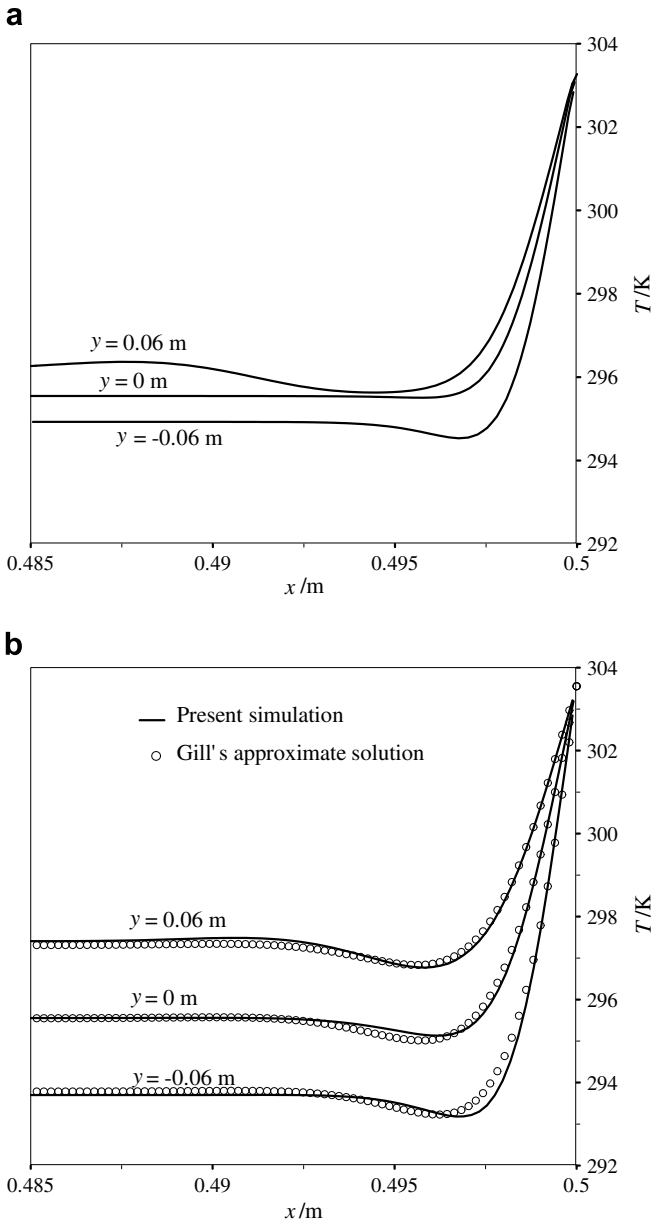

Fig. 8. Horizontal temperature profiles of the boundary layer at different heights. (a) $t = 1500$ s, and (b) $t = 4700$ s with comparison with Gill's approximate solution.

reduction in the temperature is insignificant, as shown later in Fig. 8a. Finally, at the steady state (e.g. Fig. 6, $t = 4700$ s), the stratification has extended to the mid height of the cavity and a continuous bright strip is present over the full length of the boundary layer. Note that since the development of the boundary layer and interior flows is extremely slow after $t = 4700$ (see Fig. 2a), the calculated flow at $t = 4700$ s is used for comparisons with steady analytical solutions below.

It is confirmed from the above observations that the occurrence of the temperature deficit is linked to the presence of an interior stratification, which is also possible in the transient stage. The mechanisms for these effects are different in the upper and lower half, and may be broadly described as follows. In the lower half, the boundary layer entrains fluid from the core region over the full lower half. In the part where the fluid is stratified, the interior temperature is less than the initial temperature, and the temperature difference between the core and the heated boundary layer is large. As this cold interior fluid is entrained, viscous forces take it vertically. Since $Pr > 1$, temperature diffusion into this cold fluid is slow, relative to the momentum diffusion, and the fluid remains relatively cool. Consequently, a vertical layer of cool fluid is carried up the outer edge of the boundary layer adjacent to the sidewall, resulting in the observed temperature deficit in the lower half. There is no obvious mechanism for flow reversal, and none is present in the lower half of the cavity.

In the upper half, a different mechanism is responsible for the presence of the temperature deficit. In this case, the boundary layer must detrain fluid into the core, as shown by the streamlines in Figs. 4–6. In the unstratified part, strong buoyancy effects drive the boundary layer flow upwards, and detrainment is weak. Once the interior is stratified, the effect of buoyancy is reduced as the interior temperature increases. At some height in the stratified region, the outer edge of the vertical boundary layer reaches its level of neutral buoyancy. Inertia carries it further up but eventually buoyancy forces the relatively cooler fluid to detrain and consequently fall vertically to its level of neutral buoyancy, resulting in the flow reversal and the temperature deficit. The fluid may fall too far, and a small oscillation in the vertical velocity may result, as indicated by the streamline pattern.

The mechanism outlined above may be identified in each of the Figs. 4–6. The presence of the temperature deficit in the lower part relies on the presence of a stratification in which fluid colder than the original ambient is present and is carried vertically by the boundary layer; in the upper part, the presence of a stratification means that relatively

cooler fluid on the outer edge of the boundary layer is forced to detrain but at a level at which it is negatively buoyant, resulting in both the flow reversal and the apparent temperature deficit. The flow reversal essentially occurs only in the stratified region where the boundary layer detrains; as the cold fluid detrains it is negatively buoyant and must descend.

In general terms this means that these effects are only present when there is an ambient stratification, which is also possible during the transient development of the flow. Further, the flow reversal is only strongly present when the boundary layer is detraining, that is in the upper half of the differentially heated cavity. These conclusions are clearly evident in Figs. 4–6.

Finally, the presence of the temperature deficit relies on the relatively slow diffusion of heat when compared with momentum, that is for $Pr > 1$, and may be expected to be absent, or at least greatly reduced, for $Pr < 1$. This is confirmed by many simulations for $Pr = 0.7$ [34,35].

The evolution of the temperature structure of the vertical boundary layer is shown in Fig. 8, which shows horizontal temperature profiles at different heights and different times. During the process of the development of the double-layer structure, for example at $t = 1500$ s (Fig. 8a), it is seen that the temperature profile at the middle height does not have a clear deficit, whereas deficits are clearly present in the temperature profiles of the upper and lower parts of cavity. As the boundary layer flow approaches the steady state, the stratification of the fluid in the core is further reinforced and a temperature deficit at the middle height becomes clear (Fig. 8b). These results are consistent with the mechanisms described above.

The above-mentioned horizontal temperature profile with a deficit may in turn yield a minimum and a maximum of the second derivative of the temperature with respect to the horizontal direction at the two sides of the deficit (refer to Section 4.2 for details). As mentioned in Section 3.1, the minimum and maximum second derivatives of the temperature in the x direction correspond to the two bright strips in the shadowgraph images, respectively (see Figs. 4a, 5a and 6a). Fig. 8b also shows Gill's approximate solution for the boundary layer flow, which is two-dimensional in nature (dependent on the height of the boundary layer with a stratified core in a cavity) and is clearly consistent with the present numerical solution. This implies that Gill's approximate solution characterizes well the temperature structure of the boundary layer in a differentially heated cavity with a steady stratified core (also see [35]).

4. Features of the double-layer structure

In Section 3, the formation and evolution of the double-layer structure observed in shadowgraph images are described through comparisons with the numerical simulation. It has been demonstrated that the numerical simulation is consistent with the experiment with respect to the evolution of the double-layer structure. In order to gain further insights into the double-layer structure, the flow and heat transfer properties of the double-layer structure are discussed based on numerical results in this section.

4.1. Flow features of the double-layer structure

It is seen in Fig. 6b and c that there is a small dip on the interior side of the upward thermal tongue in both the isotherm and streamline contours, which is an indication of flow reversal (also see [1–3,8]). To observe details of this flow structure, Fig. 9 shows the velocity profiles at different heights along with Gill's approximate solution. It is clear that the two solutions agree well at the higher location, but discrepancies are seen at the mid height and the lower location. This is possibly because in Gill's approximate solution of the boundary layer, advection terms in the momentum equation are neglected (refer to [3]). The difference in the Prandtl number ($Pr = \infty$ in Gill's approximation, whereas $Pr = 6.64$ in the present investigation) may also contribute to the discrepancies. Moreover, as noted previously, the numerical flow at the time of comparison ($t = 4700$ s) is not truly steady. This may also contribute to the discrepancies. Nevertheless, both solutions show the presence of flow reversal in the upper part of the cavity.

For the purpose of examining the relation between the flow and the extrema of the second derivative of the temperature in the x-direction, Fig. 10 shows a detailed view of the velocity vectors of the boundary layer and the locations of the maximum and minimum second derivatives of the temperature. The presence of flow reversal is clear here although it is much weaker than the upward flow of the inner layer. It is worth noting that the dashed lines (i.e. the lines corresponding to the minimum and maximum of the second derivatives of the temperature in the x-direction, respectively) do not correspond to the minimum and maximum of the flow velocity; that is, the bright strips in Figs. 4a, 5a and 6a do not necessarily correspond to the velocity boundary layers, although they are formed as a result of the flows.

During the formation of the double-layer structure, the change of the flow velocity magnitude is also apparent. Fig. 11a and b compare the velocity magnitudes in the vicinity of the hot wall before and after the formation of the double-layer structure. Associated with the flow transition (see Figs. 4–6), the maximum flow velocity in the boundary layer reduces as the flow reversal extends downwards, changing from approximately 0.0166 m/s in the initial stage to 0.009 m/s at $t = 4700$ s. This is consistent with the scaling result $v_{\max} \sim 0.089(g\beta\Delta TH)^{1/2}$ (giving a maximum flow velocity of 0.008 m/s for the present conditions) reported by Henkes and Hoogendoorn [36]. It is also seen in Fig. 11 that the position of the maximum velocity also moves downwards from $y = 0.1$ m near the top to approximately the middle of the cavity ($y = 0.024$ m) and closer to the hot wall, as shown in Fig. 11a and b.

Fig. 12 shows the profiles of the velocity component parallel to the heated wall and its x-direction derivatives across

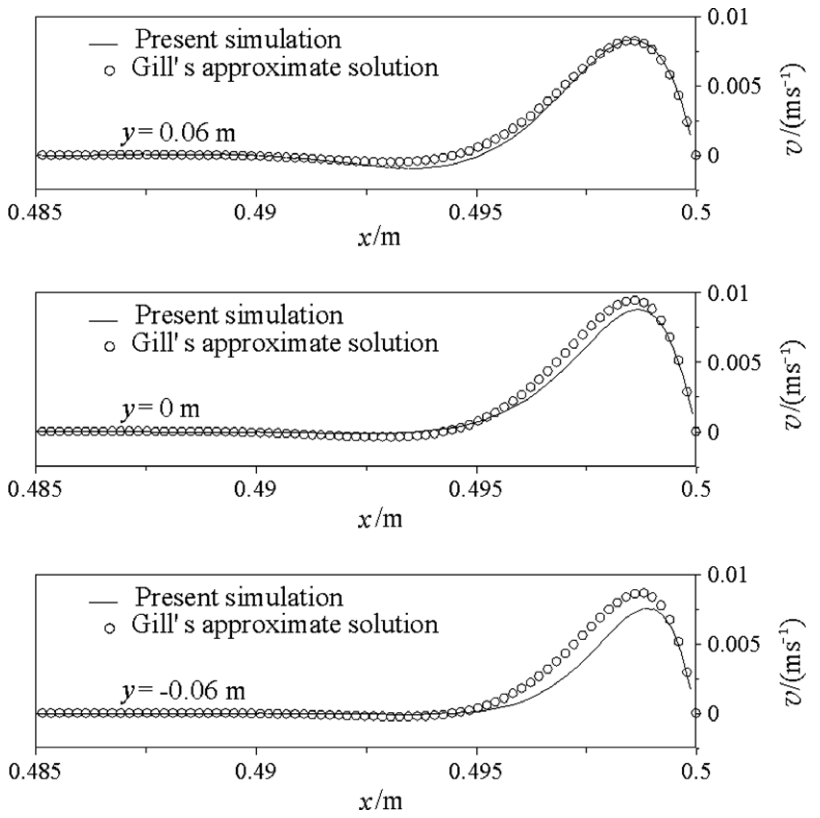

Fig. 9. Horizontal velocity profiles of the boundary layer with comparisons between Gill's approximate solution and present numerical solution at different heights at the steady stage ($t = 4700$ s).

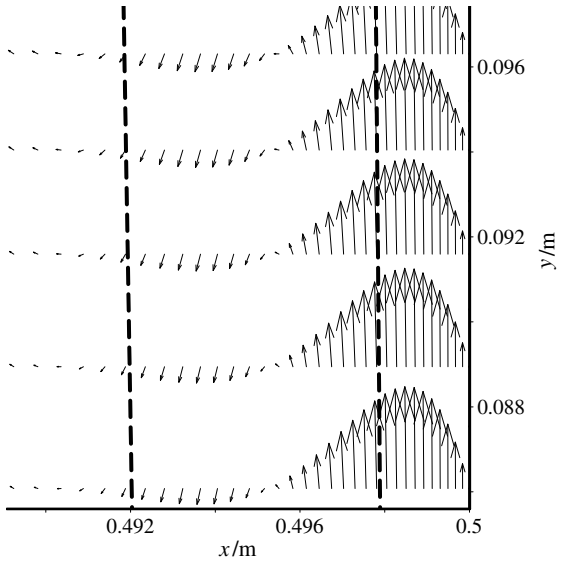

Fig. 10. Details of the velocity vector adjacent to the hot wall at the steady stage ($t = 4700$ s). The dashed lines indicate the minimum (left line) and maximum (right line) of the second derivatives of the temperature.

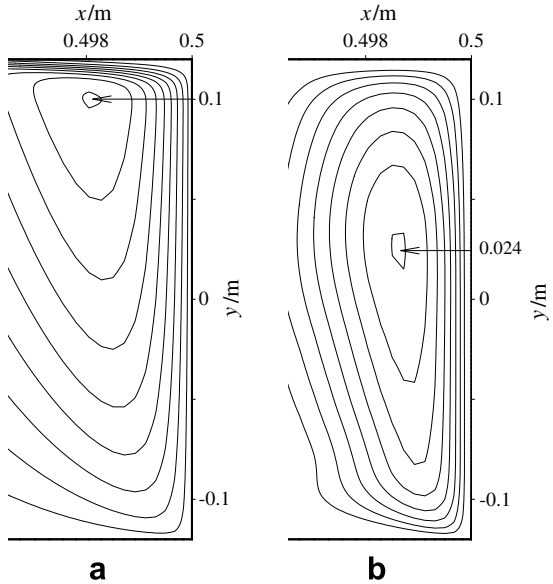

Fig. 11. Contours of the magnitude of the flow velocity adjacent to the hot wall at different times. (a) $t = 150$ s (contours between 0.0016 and 0.0166 m s^{-1} with an interval of 0.0019 m s^{-1}), and (b) $t = 4700$ s (contours between 0.002 and 0.009 m s^{-1} with an interval of 0.001 m s^{-1}).

the boundary layer at $y = 0.024$ m (where the velocity magnitude peaks at $t = 4700$ s) before and after the formation of the double-layer structure. Compared with that at the earlier stage (e.g. $t = 150$ s), the occurrence of flow reversal narrows the inner boundary layer at the later stage (e.g. $t = 4700$ s). As a result, the position of the maximum velocity in the inner boundary layer moves closer to the sidewall at the steady stage. This leads to an increase of the local shear ($\partial v/\partial x$) between the flow reversal and the inner

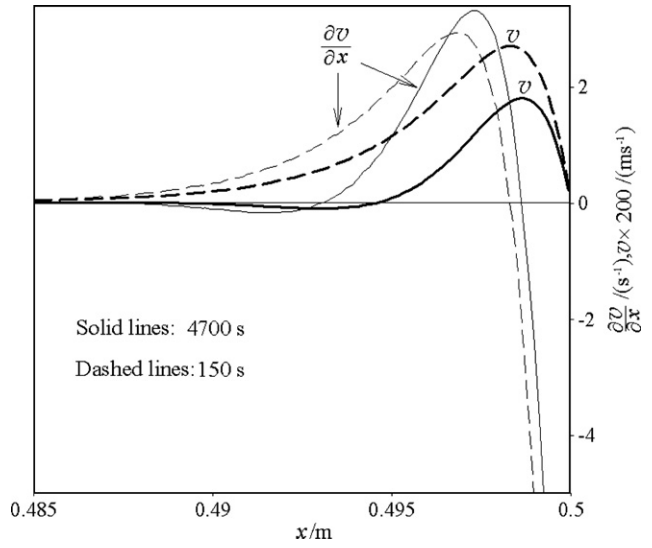

Fig. 12. Horizontal profiles of the vertical velocity component and its x-direction derivative in the double-layer structure at $y = 0.024$ m and different times.

boundary layer, as shown in Fig. 12, which shows that the maximum of the velocity derivative with respect to the x-direction at the steady stage is evidently greater than that at the earlier time. The stronger local shear is likely to be responsible for the appearance of travelling waves in the steady state boundary layer, which are observed in shadowgraph images (see Xu et al. [28]).

4.2. Heat transfer of the double-layer structure

The correspondence between the bright strips in the shadowgraph images (refer to Figs. 4a, 5a and 6a) and the maxima and minima of the second derivatives of the temperature in the direction normal to the heated wall implies that those bright strips also correspond to the positions of the maximum and minimum horizontal thermal diffusion. For the purpose of examining the horizontal thermal diffusion in the double-layer structure and its interaction with thermal convection, the energy equation (Eq. (4)), subject to the usual boundary layer assumptions, is rewritten for the steady state boundary layer flow as

$$\kappa\frac{\partial^2 T}{\partial x^2} + \left(-u\frac{\partial T}{\partial x}\right) + \left(-v\frac{\partial T}{\partial y}\right) = 0. \tag{5}$$

Eq. (5) describes, in a differential sense, the heat balance between thermal diffusion ($\kappa\partial^2 T/\partial x^2$) and convection (horizontal component – $u\partial T/\partial x$ and vertical component – $v\partial T/\partial y$) in a control element near the wall. If the value of a certain term is positive, the term contributes heat to the control element, whereas a negative term results in a net loss of heat from the control element. As previously indicated (also see Fig. 2a), the development of the vertical boundary layer adjacent to the sidewall is extremely slow after $t = 4700$ s, the boundary layer at $t = 4700$ s is assumed to be at the steady state. Fig. 13 plots the horizontal profiles of the temperature, velocity and the different terms of Eq. (5) at $t = 4700$ s for two different locations along the heated wall ($y = 0.06$ m and -0.06 m, representing the upper and lower parts of the double-layer structure, respectively). In this figure, the vertical dashed lines indicate the positions of the minimum and maximum of the horizontal thermal diffusion (corresponding to the positions of the bright strips in the shadowgraph images), and the vertical solid lines indicate the positions of the minimum temperature (i.e. the temperature deficit). The three vertical lines divide the flows adjacent to the sidewall into four regions with Region I corresponding to the inner layer referred to previously and Regions II and III constituting the outer layer (refer to Fig. 13).

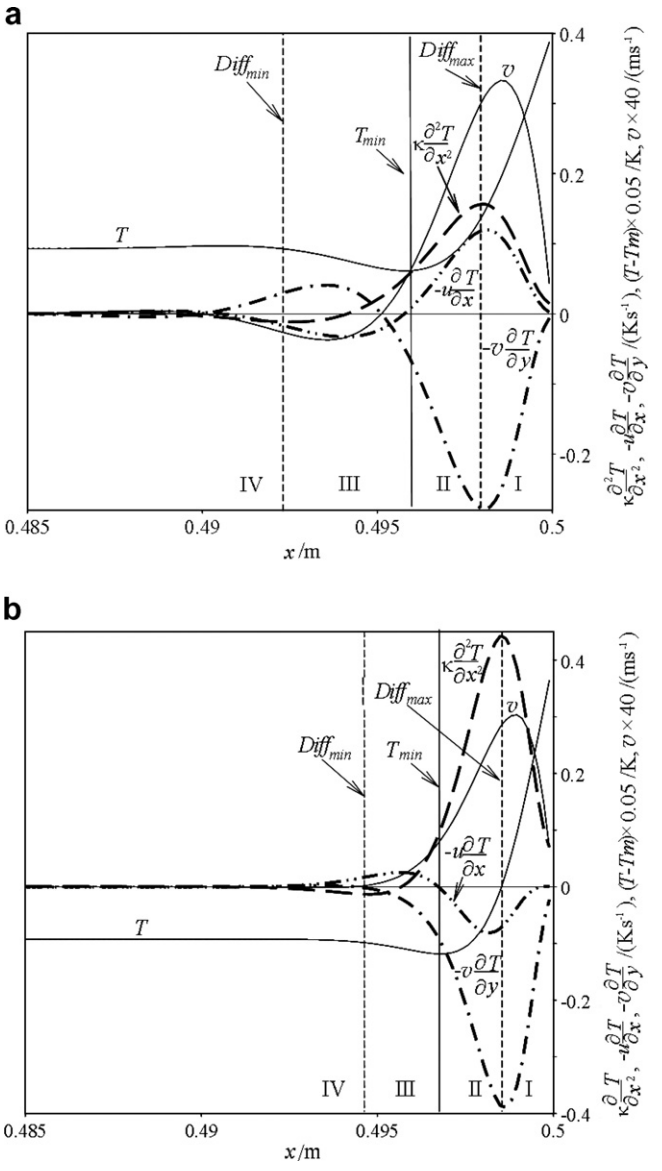

Fig. 13. Horizontal profiles of the thermal diffusion and convection terms in the double-layer structure at $t = 4700$ s. $Diff_{min}$, $Diff_{max}$ and T_{min} denote the minimum thermal diffusion, maximum thermal diffusion and minimum temperature, respectively. (a) $y = 0.06$ m, and (b) $y = -0.06$ m.

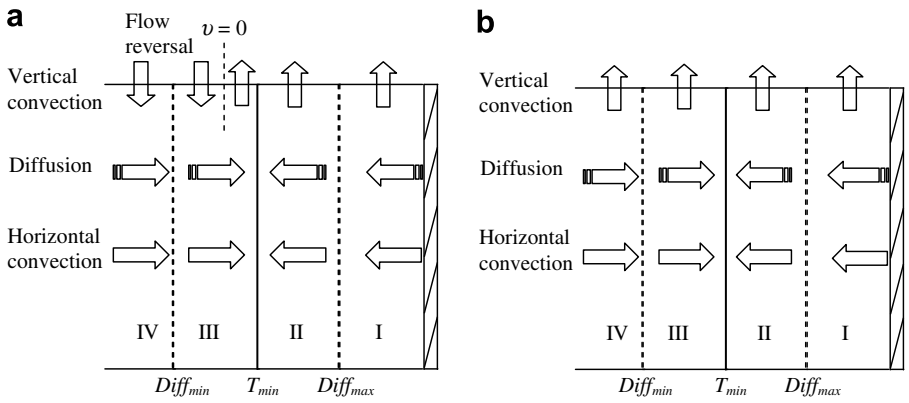

Fig. 14. Schematics showing the heat transfer by different modes in various regions at the steady stage. (a) Schematic corresponding to the profiles at $y = 0.06$ m (Fig. 13a) in the upper section of the cavity, and (b) schematic corresponding to the profiles at $y = -0.06$ m (Fig. 13b) in the lower section of the cavity.

It is seen in Fig. 13 that, for both the upper and lower parts of the cavity, both thermal diffusion and convection increase with the distance from the wall in Region I. Outside Region I, all terms in Eq. (5) reduce significantly with the increasing distance from the heated wall.

For the upper section of the cavity, Fig. 13a shows that, in Region I, vertical thermal convection takes away the heat transferred into the region by thermal diffusion and horizontal convection from the hot wall. Due to the stratification of the interior flow at this time, thermal diffusion is relatively weak in the upper section, and horizontal convection from the hot wall is comparable with thermal diffusion. In Region II, the heat balance is similar to that in Region I. Although the heat transfer beyond the point of the temperature minimum significantly reduces, it is worth noting a feature of interest regarding the direction of thermal diffusion on either side of the temperature minimum. Clearly, thermal diffusion in Regions I and II is directed from the sidewall towards the interior, whereas in Regions III and IV, thermal diffusion is directed from the interior towards the minimum.

Compared to the flow in the upper section of the cavity, thermal diffusion and vertical convection in the lower cavity are much stronger due to the stratification of the interior flow. Horizontal convection remains at approximately the same order as in the upper section but with an opposite sign. This term is less significant compared with the thermal diffusion and vertical convection terms. Fig. 13b shows that, in the lower section of the cavity, the heat balance in Region I is mainly between thermal diffusion from the hot wall and vertical convection. This heat balance extends to the point of the temperature minimum, beyond which heat transfer becomes very weak. The opposing thermal diffusion at the point of the temperature minimum is also present in the lower section. In fact, since there exists a temperature minimum, heat cannot be diffused beyond the temperature minimum point and thus is taken away completely by convection.

In order to illustrate clearly the heat flow in different regions, based on the above discussion, schematics of the heat transfer in the upper and lower sections of the cavity are shown in Fig. 14a and b, respectively. It is clear that thermal diffusion is opposing between Regions II and III (separated by the temperature minimum) in both the upper and lower parts of the cavity. Although horizontal convection in the upper section is directed to the interior (due to detrainment of the boundary layer), the heat fluxes resulting from horizontal convection are opposing on the two sides of the temperature minimum (Fig. 14a). The same effect of horizontal convection may be found in the lower section (Fig. 14b) with the heat flux opposing the horizontal flow in Regions I and II as a consequence of relatively colder fluid is taken to the region. It is seen in Fig. 14b that vertical convection in the lower section of the cavity is directed upwards. However, in the upper section of the cavity, it changes direction due to the flow reversal in the outer layer (Fig. 14a).

In summary, heat transfer in the upper and lower sections of the cavity is complex, with the role of the horizontal convection changing between the two sections. A transitional region is expected to be present near the mid height, where the horizontal velocity changes its direction.

5. Conclusions

In this paper, the transition of the boundary layer adjacent to the sidewall of a differentially heated cavity to a double-layer structure is characterized, and the mechanism responsible for the formation of the double-layer structure is discussed based on combined experimental and numerical investigations. The numerical simulation is consistent with the experimental observation.

The results have demonstrated that a double-layer structure of the boundary layer observed in shadowgraph images simultaneously develops from the top and bottom, respectively. In the upper part of the cavity, the outer bright strip develops from the detrainment of the boundary layer. In the meantime, in the lower part of the cavity a similar outer bright strip develops from entrainment of the incoming cold intrusion. The two branches of the outer bright strips eventually meet at the mid height and align vertically, forming a

continuous double-layer structure with a slightly increasing thickness over the length of the vertical boundary with height. It has been demonstrated that the inner and outer bright strips observed in shadowgraph images approximately correspond to the maximum or minimum of the second derivatives of the temperature (see e.g. Figs. 4–6, 10 and 13), and the mechanism responsible for the formation of the double-layer structure of the boundary layer is the stratification of the interior fluid in the core.

In the steady stage, the flow in the double-layer structure is complex, which includes an inner boundary layer adjacent to the hot wall and flow reversal outside the inner layer with a stronger local shear in the upper part of the cavity, as seen in Fig. 12. Due to the presence of the strong shear, the double-layer structure is considered as a potential cause responsible for the appearance of the unstable travelling waves observed in shadowgraph images [28].

The present numerical results also indicate that heat transfer near the wall is rather complex, and significantly depends on the development of the flow. After the formation of the double-layer structure, a deficit of the temperature profile adjacent to the hot wall appears, resulting in opposing horizontal thermal diffusion on the two sides of the temperature deficit; that is, thermal diffusion is directed toward the temperature deficit on both sides. This implies that the heat from the hot sidewall cannot be diffused beyond the location of the temperature minimum, which may thus be considered as an 'insulation wall' blocking thermal diffusion.

Acknowledgement

The authors are grateful for the financial support of the Australian Research Council.

References

[1] L. Prandtl, Essentials of Fluid Dynamics, Blackie, London, 1952, pp. 422–425.
[2] J.W. Elder, Laminar free convection in a vertical Slot, J. Fluid Mech. 23 (1965) 77–98.
[3] A.E. Gill, The boundary-layer regime for convection in a rectangular cavity, J. Fluid Mech. 26 (1966) 515–536.
[4] G.K. Batchelor, Heat transfer by free convection across a closed cavity between vertical boundaries at different temperatures, Quart. Appl. Math. 12 (1954) 209–233.
[5] E.R.G. Eckert, W.O. Carlson, Natural convection in an air layer enclosed between two vertical plates at different temperatures, Int. J. Heat Mass Transfer 2 (1961) 106–120.
[6] J. Tao, P. Le Quere, S. Xin, Absolute and convective instabilities of natural convection flow in boundary-layer regime, Phys. Rev. E 70 (2004) 066311.
[7] J. Tao, P. Le Quere, S. Xin, Spatio-temporal instability of the natural-convection boundary layer in thermally stratified medium, J. Fluid Mech. 518 (2004) 363–379.
[8] A. Shapiro, E. Fedorovich, Unsteady convectively driven flow along a vertical plate immersed in a stable stratified fluid, J. Fluid Mech. 498 (2004) 333–352.
[9] A. Shapiro, E. Fedorovich, Natural convection in a stably stratified fluid along vertical plates and cylinders with temporally periodic surface temperature variations, J. Fluid Mech. 546 (2006) 295–311.
[10] R. Siegel, Transient free convection from a vertical flat plate, J. Heat Transfer 80 (1958) 347–360.
[11] R.J. Goldstein, D.G. Briggs, Transient free convection about vertical plates and cylinders, J. Heat Transfer 86 (1964) 490–500.
[12] B. Gebhart, Transient response and disturbance growth in vertical buoyancy-driven flows, J. Heat Transfer 110 (1988) 1166–1174.
[13] S.W. Armfield, J.C. Patterson, Wave properties of natural convection boundary layers, J. Fluid Mech. 239 (1992) 195–212.
[14] J.C. Patterson, T. Graham, W. Schöpf, S.W. Armfield, Boundary layer development on a semi-infinite suddenly heated vertical plate, J. Fluid Mech. 219 (2002) 467–497.
[15] J.A. Schetz, R. Eichorn, Unsteady natural convection in the vicinity of a doubly infinite vertical plate, J. Heat Transfer 84 (1962) 334–338.
[16] S. Ostrach, Laminar flows with body forces, in: F.K. Moore (Ed.), Theory of Laminar Flows, Princeton University Press, 1964.
[17] S.N. Brown, N. Riley, Flow past a suddenly heated vertical plate, J. Fluid Mech. 59 (1973) 225–237.
[18] R.L. Mahajan, B. Gebhart, Leading edge effects in transient natural convection flow adjacent to a vertical surface, J. Heat Transfer 100 (1978) 731–733.
[19] Y. Joshi, B. Gebhart, Transition of transient vertical natural-convection flows in water, J. Fluid Mech. 179 (1987) 407–438.
[20] S.G. Schladow, Oscillatory motion in a side-heated cavity, J. Fluid Mech. 213 (1990) 589–610.
[21] J.C. Patterson, J. Imberger, Unsteady natural convection in a rectangular cavity, J. Fluid Mech. 100 (1980) 65–86.
[22] G.N. Ivey, Experiment on transient natural convection in a cavity, J. Fluid Mech. 144 (1984) 389–401.
[23] S. Paolucci, D.R. Chenoweth, Transition to chaos in a differentially heated vertical cavity, J. Fluid Mech. 201 (1989) 379–410.
[24] P. Le Quere, Transition to unsteady natural convection in a tall water-filled cavity, Phys. Fluids 2 (1990) 503–515.
[25] M.R.R. Ravi, R.A.W.M. Henkes, C.J. Hoogendoorn, On the high-Rayleigh-number structure of steady laminar natural-convection flow in a square enclosure, J. Fluid Mech. 262 (1994) 325–351.
[26] S.G. Schladow, J.C. Patterson, R.L. Street, Transient flow in a side-heated cavity at high-Rayleigh number: a numerical study, J. Fluid Mech. 200 (1989) 121–148.
[27] S.W. Armfield, J.C. Patterson, Direct simulation of wave interactions in unsteady natural convection in a cavity, Int. J. Heat Mass Transfer 34 (1991) 929–940.
[28] F. Xu, J.C. Patterson, C. Lei, Shadowgraph observations of the transition of the thermal boundary layer in a side-heated cavity, Exp. Fluid 38 (2005) 770–779.
[29] J.M. Hyun, Transient process of thermally stratifying initially homogeneous fluid in an enclosure, Int. J. Heat Mass Transfer 27 (1984) 1936–1938.
[30] W. Lin, S.W. Armfield, Natural convection cooling of rectangular and cylindrical container, Int. J. Heat Fluid Flow 22 (2001) 72–81.
[31] J.C. Patterson, S.W. Armfield, Transient features of natural convection in a cavity, J. Fluid Mech. 219 (1990) 469–497.
[32] W. Schöpf, J.C. Patterson, Natural convection in a side-heated cavity: visualization of the initial flow features, J. Fluid Mech. 295 (1995) 279–357.
[33] W. Merzkirch, Flow Visualization, Academic Press, 1974.
[34] H.S. Dol, K. Hanjalic, Computational study of turbulent natural convection in a side-heated near-cubic enclosure at a high-Rayleigh number, Int. J. Heat Mass Transfer 44 (2001) 2323–2344.
[35] R.A.W.M. Henkes, Natural-Convection boundary layers, Ph.D thesis, the Delft University of Technology, 1990.
[36] R.A.W.M. Henkes, C.J. Hoogendoorn, Scaling of the laminar natural-convection flow in a heated square cavity, Int. J. Heat Mass transfer 36 (1993) 2913–2925.